Plasma Facing Component Characterization and Correlation With Plasma Conditions in Lithium Tokamak Experiment-β

Anurag Maan, Evan Ostrowski, Robert Kaita, David Donovan, Richard Majeski, Dennis Boyle, Paul Hughes, Enrique Merino, Tom Kozub, Bruce E. Koel, Drew Elliott, Theodore Biewer, Filippo Scotti, Vsevolod Soukhanovskii, and Robert Lunsford

***Abstract*— Lithium coatings in the Lithium Tokamak eXperiment (LTX) led to flat temperature profiles. The flat temperature profiles were observed along with a hot, low density edge, implying a broad, collisionless scrape-off layer (SOL). Additionally, in vacuo X-ray photoelectron spectroscopy (XPS) measurements established that lithium coatings evaporatively deposited onto high-Z plasma facing components (PFCs) became oxidized while retaining the ability to achieve good plasma performance long after lithium was applied to the PFCs. Longstanding theory predicted flat temperature profiles with low recycling walls, which was presumed to be due to hydrogen binding with elemental lithium to form lithium hydride. The presence of oxidized lithium, however, raised questions regarding the exact mechanism of hydrogen retention in LTX. To investigate these questions, the upgraded facility LTX-β includes a new sample exposure probe (SEP) for more detailed in vacuo analysis of PFC samples. The SEP is equipped with a vacuum suitcase capable of transporting samples representative of the LTX-β outer midplane PFCs to a stand-alone XPS system while maintaining pressures lower than the LTX-β base vacuum to limit the contamination between sample exposure and analysis. The low-energy resolution XPS system used in past experiments could only enable the determination of elemental percentages on the PFC sample surfaces. Because the new XPS system has higher energy resolution, it is more direct to assign chemical compounds to the measured binding energies. This capability has been confirmed by comparing XPS data from PFC test samples with measurements using a commercial high-resolution XPS system. Quartz crystal microbalances (QCMs) were used to quantify the thickness of the deposited lithium on the LTX-β PFCs. This article describes the application of the SEP to characterize the PFC surfaces using XPS and their relationship to plasma conditions.**

***Index Terms*— Lithium, plasma chemistry, plasma confinement, plasma diagnostics, tokamaks.**

Manuscript received July 19, 2019; revised January 2, 2020; accepted January 18, 2020. This work was supported by the U.S. DOE under Grant DE-AC02-09CH11466, Grant DE-AC05-00OR22725, Grant DE-AC52-07NA27344, and Grant DE-SC0019308. The review of this article was arranged by Senior Editor G. H. Neilson. *(Corresponding author: Anurag Maan.)*

Anurag Maan, Robert Kaita, and David Donovan are with the Department of Nuclear Engineering, University of Tennessee, Knoxville, TN 37996 USA (e-mail: amaan@vols.utk.edu).

Evan Ostrowski and Bruce E. Koel are with the Chemical and Biological Engineering, Princeton University, Princeton, NJ 08544 USA.

Richard Majeski, Dennis Boyle, Paul Hughes, Enrique Merino, Tom Kozub, and Robert Lunsford are with the Princeton Plasma Physics Laboratory, Princeton, NJ 08540 USA.

Drew Elliott and Theodore Biewer are with the Oak Ridge National Laboratory, Oak Ridge, TN 37831 USA.

Filippo Scotti and Vsevolod Soukhanovskii are with the Lawrence Livermore National Laboratory, Livermore, CA 94550 USA.

Color versions of one or more of the figures in this article are available online at http://ieeexplore.ieee.org.

Digital Object Identifier 10.1109/TPS.2020.2969115

I. Introduction

THE choice of materials for the first wall inside a tokamak, also called the plasma facing components (PFCs), has major engineering and physics implications for the overall design. Empirically, it has been shown that the use of high-Z PFCs lowers confinement in JET [1]. It has also been observed that the use of low-Z PFCs, especially lithium, improves plasma performance in various machines, including TFTR, NSTX, CDX-U, and EAST [2]–[6]. One of the primary objectives of the Lithium Tokamak eXperiment (LTX) and its upgrade LTX-β is to investigate lithium as a PFC coating on a high-Z substrate in order to improve plasma performance. LTX is a spherical tokamak at the Princeton Plasma Physics Laboratory (PPPL) with a cylindrical vacuum vessel of dimensions 0.9 m height and 1.4 m inner diameter. Inside the vessel are stainless-steel-clad copper shells designed to be conformal to a plasma with major radius $R = 0.4$ m, minor radius $a = 0.26$ m (aspect ratio $A = 1.6$), and maximum elongation $\kappa \approx 1.5$ [7]. LTX operated with a toroidal field ≈ 1.7 kG, $I_p \leq 80$ kA, and a short duration of ≤ 25 ms. The facility was upgraded to LTX-β with nearly double the field and the addition of a neutral beam.

During its final campaign, LTX was fueled by gas puffs from the high field side. Once the fueling was terminated, Thomson Scattering measurements showed that the electron temperature profiles flattened. Although recycling was not measured directly, pressure measurement of the fueling gas before, during, and after the discharge indicated significant wall retention [8]. The LTX results were the first experimental observation of near-zero temperature gradient profiles attributed to low recycling PFCs. In addition, experimentally measured energy confinement exceeded the predictions for ohmic plasmas by a factor of $\sim$3 [8].

The materials analysis and particle probe (MAPP), designed to characterize PFC surfaces in vacuo (i.e., without any exposure to air) was first used on LTX. The samples were inserted to be flush with the plasma facing surfaces of the conducting

shells [9], [10]. Samples on the probe head included those made of stainless steel (SS-304 and SS-316) to match the LTX shell surfaces. The LTX shells and samples were then coated with lithium, after which the probe head was exposed to LTX plasma. Post exposure, the probe was retracted in vacuo into the MAPP analysis chamber for X-ray photoelectron spectroscopy (XPS) determination of the surface composition of the lithium coated SS-304 MAPP sample. XPS indicated an increase in the oxygen concentration of the sample after exposure to LTX residual vacuum conditions, which was attributed to oxidation by water vapor that was observed by the residual gas analyzer (RGA).

The temporal evolution of lithium and oxygen concentrations were also tracked using MAPP. It was observed that the Li(1s)/O(1s) ratio decreased, until it saturated the XPS probe depth, within 5 h [9], [10]. Beyond that, there was no observable change in the elemental concentration until 100 h, after which the Li(1s)/O(1s) ratio began to decrease slowly. The saturation of the ratio of lithium to oxygen to about 2:1 was attributed to the growth of Li_2O on freshly deposited lithium in the presence of residual water vapor, consistent with laboratory experiments [11], [12]. Specifically, below 100 Langmuirs (1 $L = 10^{-6}$ torr·s) of H_2O exposure, Li_2O forms preferentially on a clean lithium surface, while at higher exposures there is a transition to LiOH formation. For LTX-relevant water partial pressures, 100 L is equivalent to 14 h of exposure to residual vacuum. It was also observed that the presence of the oxide did not degrade plasma performance; LTX continued to get high plasma currents until 40 days after lithium deposition [6].

About 0.5 s after the plasma extinguished in LTX, the fast ion gauge showed a ∼60% reduction in H_2 inventory compared to calibration gas puffs where plasma was not initiated [6], [8]. Over longer (>10 s) timescales, however, the H_2 reading from the RGA for shots when plasma was initiated exceeded the recorded measurement for the calibrated gas puffs. This led to the conclusion that while a significant portion of hydrogen was retained in the PFCs during a plasma, the hydrogen out-gassed over time scales much longer than the plasma duration [6]. With 60% of an LTX relevant fluence of hydrogen fuel retained in a lithium coating of 100 nm, the Li coating should saturate with hydrogen in <10 shots (assuming Li:H = 1:1). However, this was not the case. Neither H retention nor plasma performance decayed after a few shots, but rather after 40 days and close to one hundred shots or more. This led to the conclusion that hydrogen was retained by lithium-coated PFCs in LTX such that it was free to diffuse out between shots. The conclusions regarding the state of the PFC using MAPP results were arrived at using elemental abundances only. Binding energy shifts using XPS can be used to identify chemical states, but MAPP did not have the energy resolution to identify different Li compounds that formed on the PFCs.

II. Upgrade to LTX-β

The upgrade to LTX-β included the ability to operate at higher fields and with more efficient Li evaporators

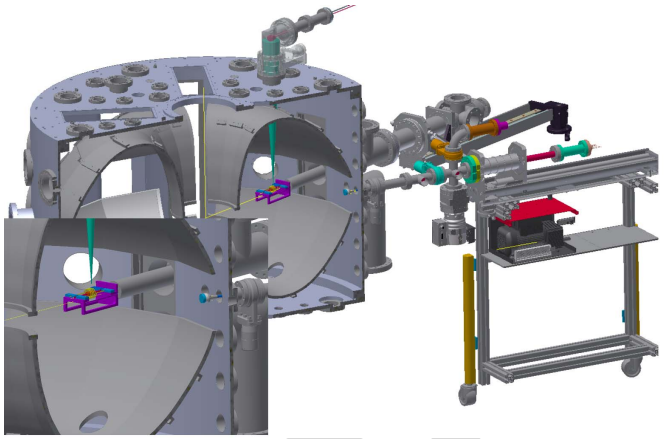

Fig. 1. CAD section view of the evaporator inserted to the central poloidal location, the SEP, and the QCM above the LTX-β vacuum vessel. Also visible are the stainless-steel-clad copper shells inside the vacuum vessel. Inset: zoomed-in view of the evaporator subassembly and trajectory of lithium vapor toward the QCM.

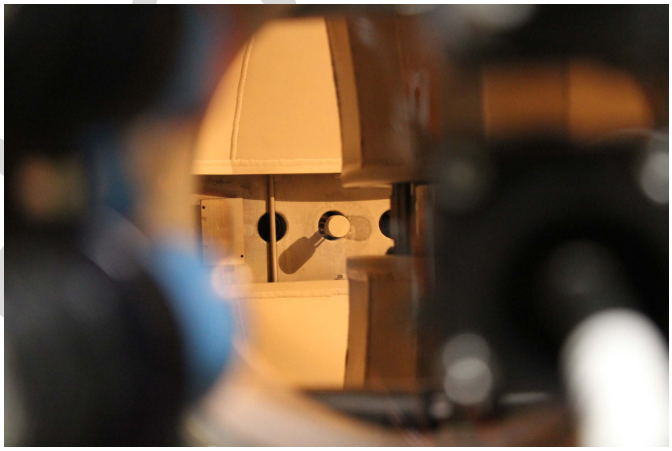

Fig. 2. SEP probe head immediately after lithium evaporation. The probe head face is flush with the inner face of the LTX-β shells. Two shadows from the SEP probehead are visible, the shadow to the bottom-left of the probe is cast by an in-vessel filament that is illuminating the vessel interior, the shadow to the right is cast by the lithium evaporator.

(see Fig. 1). The machine has been operated with 600 kW of neutral beam injection and several hundred nanometers of lithium coatings [13]. Fig. 3 illustrates the main plasma parameters of a wide variety of discharges through the upgrade campaign. It was observed that the discharges grew longer and had higher plasma current after lithium evaporation. In Fig. 3, lithium PFC discharges are divided into two groups. Discharges after the first lithium evaporation (represented by green bubbles in Fig. 3) had higher electron density, but were shorter in duration with lower plasma current. Discharges after subsequent lithium evaporations (represented by red bubbles in Fig. 3) could achieve longer durations and higher currents. Spectroscopic data indicated a reduction in carbon and oxygen impurities and an increase in lithium line emission when discharges were initiated after a fresh coat of lithium [13].

Each of the LTX-β lithium evaporators consists of a basket made of stainless steel mesh, suspended through two yttria

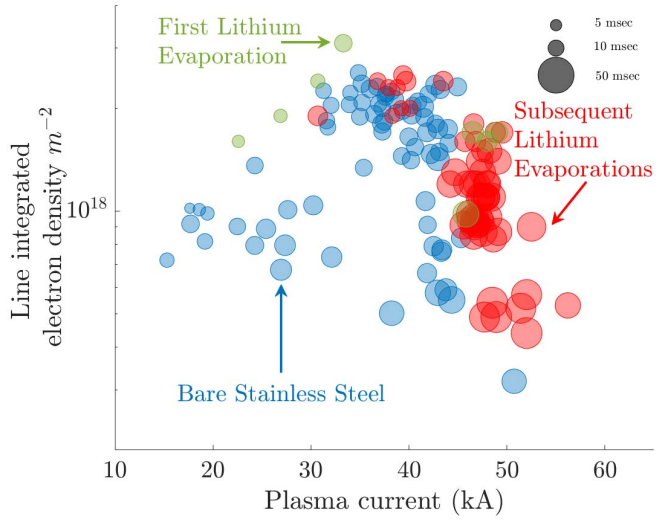

Fig. 3. Line integrated electron density as a function of plasma current for LTX-β discharges; bubble size is proportional to plasma current flat-top duration of 4–40 ms. Discharges with bare stainless steel walls are shown in blue; discharges after the first lithium evaporation are shown in green, and after subsequent lithium evaporations are shown in red.

TABLE I
CHRONOLOGY OF LITHIUM EVAPORATION EVENTS ON LTX-β

Days*	Li thickness QCM (nm)	Estimated Li on SEP (nm)
30.6	22	89.5
31.7	7	28.5
37.5	108	439.5
41.8	50.8	206.7
44.5	40	162.8

*Days from the first XPS measurement as referred in Fig 4.

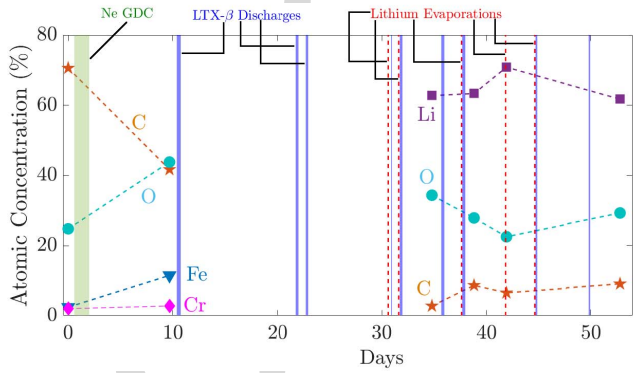

Fig. 4. Elemental concentrations measured using the SEP. Vertical green bar: neon glow discharge duration. Vertical blue bars: time duration over which LTX-β discharges were initiated. Dashed red lines: lithium evaporations on the shells and SEP.

rods for support. Evaporator temperatures are measured with a Type-K thermocouple inserted into one of the yttria rods [13]. The basket is surrounded by a tungsten coil heater that can be quickly ramped up to 60 A (~500 W) to radiatively heat the lithium pieces loaded in the basket. The lithium pieces are pre-cut and loaded into a stainless steel container in an argon glovebox for transfer under argon. Lithium evaporators are back-filled with dry argon and lithium coupons carefully transferred into the evaporator from the container. A slight outflow of argon from the evaporator assembly is maintained, thereby minimizing the exposure of lithium to the atmosphere. LTX-β has two evaporators installed in diametrically opposite toroidal locations to provide near full coverage of PFCs by lithium coatings. Once lithium is loaded, the evaporators are pumped out and inserted into LTX-β, such that they are at the center of their respective poloidal planes as shown in Fig. 1. Each evaporator is situated under a shell penetration that provides a line of sight to a quartz crystal microbalance (QCM). The QCMs are used to keep track of lithium deposited per evaporation.

Simultaneously, the sample exposure probe (SEP) is inserted to be flush with the plasma facing side of the shells (see Fig. 2). The SEP is left in this position for lithium evaporations and subsequent plasma discharges. This article analyzes five such lithium evaporation events (Table I). The lithium deposited per evaporation is recorded by the QCM; these recorded values can be used to estimate the thickness of lithium deposited on the SEP using the expressions for evaporative flux [14]. Assuming the evaporator sub-assembly to be a point source, the lithium thickness on the SEP can be estimated by (1), where t_{SEP} is the thickness of lithium on the SEP, t_{QCM} is the lithium thickness measured by the QCM, θ is the angle from the point source to the SEP surface normal, r_{QCM} is the distance from the QCM to the evaporator source and r_{SEP} is the distance of the evaporator source to the SEP

$$t_{SEP} = t_{QCM}\cos(\theta)\frac{r_{QCM}^2}{r_{SEP}^2}. \quad (1)$$

Once the desired exposure of residual vacuum or plasma discharges is achieved, the SEP is removed from LTX-β and moved to the Surface Science and Technology Laboratory (SSTL) at PPPL where it is docked to an ultrahigh vacuum (UHV) system that has a XPS spectrometer [15]. The transfer is made within a limited time (<1.5 h), such that the fluence of impurities on the surface is similar to a MAPP scan [15].

III. ENHANCED SURFACE ANALYSIS CAPABILITIES

Prior to the introduction of lithium, surface conditioning for LTX-β involved Ne glow discharge conditioning (GDC) and simultaneous high temperature shell's bake at 250 °C. To ensure that the SEP sample head accurately represented the LTX plasma facing shells, the SEP was inserted flush with shells during GDC and bake and was maintained at the same temperature as the shells. Surface elemental composition was measured using XPS before and after the GDC (see Fig. 4). It was observed that the elemental concentration of C declined while the concentrations of Fe and O went up; this is attributed to the sputtering of the adventitious carbon by Ne, which would result in the underlying iron oxides to appear more intense on the XPS scan. The sampling depth is expected to be about 6 nm [15]. For these measurements, the SEP is left exposed inside LTX-β except for the brief intervals during which it is taken off for taking XPS scans. Following the first lithium evaporation and subsequent LTX-β discharges, surface

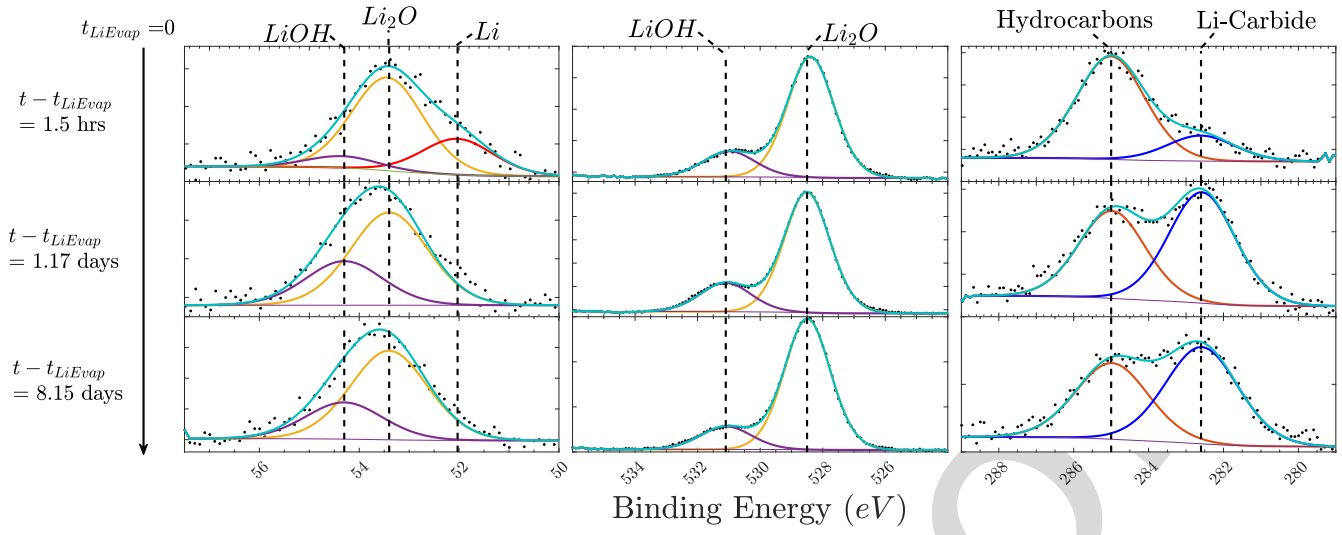

Fig. 5. Narrow band regional XPS scans for Li(1s), O(1s), and C(1s) along with probable fits are shown in left, middle, and right columns, respectively. The scans are arranged row-wise in increasing order of time from a lithium evaporation.

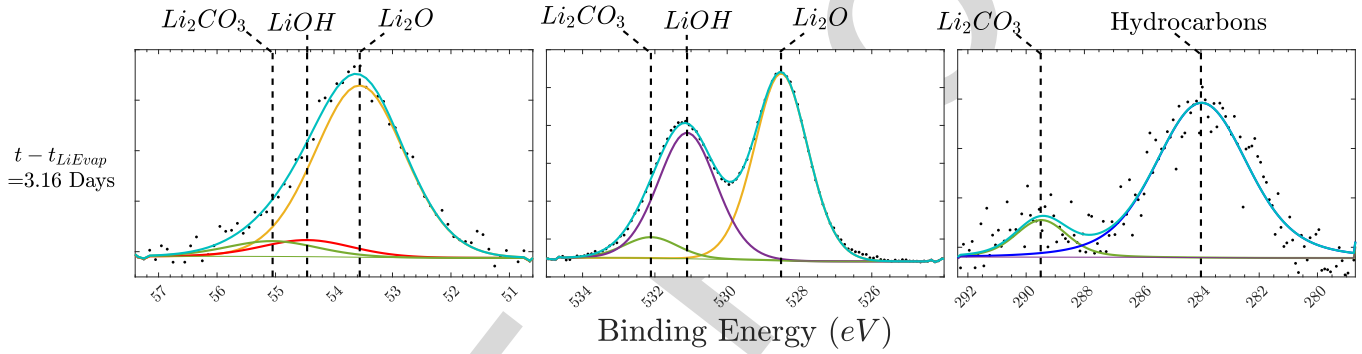

Fig. 6. Narrow-band regional XPS scans along with probable fits for Li(1s), O(1s), and C(1s) are shown in left, middle, and right columns, respectively. The scan was taken 3.16 days after lithium was deposited on bare stainless steel walls and sample head of the SEP.

concentrations were measured again; the measurements show that the stainless steel substrate of the SEP was completely covered by lithium. XPS measurements made for relatively fresh lithium coatings show higher Li and lower O concentrations; as the surface accumulates LTX-β residual vacuum exposure time, the O concentration seems to climb up, and Li concentration is seen to decrease relative to O.

A. Surface Chemical Species Identification Using the SEP

Coupled with the XPS system at SSTL, the SEP enabled chemical identification of species present on the surface. Figs. 5 and 6 represent the regional narrow band scans collected for the samples whose elemental compositions are shown in Fig. 4. Similar studies have been performed for boronized NSTX-U PFCs [16] and have enabled identification of oxygen retention mechanisms that resulted in improved plasma performance.

The O(1s) peak, shown in the middle column of Fig. 5, exhibited two features that were identified to be Li_2O and LiOH at the binding energies of 528.5 and 531.1 eV, respectively. The absolute values of these binding energies and the difference between them is consistent with results cited elsewhere [17], [18]. The O(1s) Li_2CO_3 peak was identified to be at 532.1 eV [17]–[19] for measurements that were taken after the first application of lithium on steel PFCs of LTX-β (see Fig. 6). All peaks are referenced to a hydrocarbon peak in the C(1s) region at 285 eV. An additional feature in the C(1s) region at 282.6 eV is attributed to lithium carbide with reference to the hydrocarbon peak at 285 eV; this assignment is consistent with values in the literature [20]. The higher energy feature in the C(1s) region visible in Fig. 6 at 289.4 eV is attributed to Li_2CO_3. The Li(1s) region in both Figs. 5 and 6 was fit with peaks at 52.03, 53.4, 54.3, and 55 eV for Li, Li_2O, LiOH, and Li_2CO_3, respectively. The difference in binding energies of these fits was forced to be consistent with values reported in the literature [12], [17], [19].

The narrow region scans elaborate on the richness of surface chemistry of evaporative lithium coatings on PFCs. The surface chemistry is both a function of tokamak residual vacuum and plasma exposures and is expected to be similar across machines that employ lithium coatings. However, the rate of growth of these species will be dependent on each machine's residual vacuum and plasma exposure conditions. The O(1s) region indicates that the primary lithium species on the PFCs is Li_2O followed by LiOH. The first application of lithium,

as shown in Fig. 6, however, appears to result in the formation of Li_2CO_3 and LiOH in addition to Li_2O, and this was observed along with plasma performance that was moderate in comparison to performance after a few more evaporations, as witnessed by an increase in plasma current and density (see Fig. 3). This is likely a result of vacuum and PFC surface conditions being different from samples represented in Fig. 5, for which lithium was evaporated on already lithiated PFCs. The carbonate production is likely a result of adventitious carbon on the stainless steel surface, which although reduced in magnitude after GDC, was still amongst the two largest elemental constituents of the steel PFCs.

Two novel observations can be made about lithium PFCs that consist of evaporative lithium coatings. First is the formation and growth of lithium carbide, as can be seen in the C(1s) regional scan in Fig. 5. The second is the presence of a relatively large elemental lithium peak in row 1 and column 1 of Fig. 5. The presence of elemental lithium indicates that the oxide grows on top of lithium deposited during evaporation events.

IV. Conclusion

The chemical evolution of lithium coated evaporatively on stainless steel PFCs was tracked through surface conditioning, lithium deposition, and plasma discharge events. This was made possible due to a SEP that enabled the UHV transfer of samples to a dedicated XPS system with resolution that was sufficient to identify chemical species. The results support the hypothesis that for evaporative coatings of lithium under low-water content residual vacuum, Li_2O grows before transitioning to LiOH. We further hypothesize that the first few lithium evaporations of a few hundred nanometers in total on LTX-β shells were able to limit carbon uptake in subsequent lithium coatings from underlying stainless steel. The first lithium coating consisted of relatively large hydroxide and carbonate components in addition to Li_2O. The hydroxide and carbonate in the coating are likely a result of the interaction of lithium from the first deposition with the underlying carbon and oxygen on the steel. Subsequent lithium evaporations likely bury these species such that these later coatings manifest as mostly Li_2O on lithium. The presence of elemental lithium seen in freshly deposited lithium coatings indicates limited oxygen codeposition with lithium and hint at an ordered growth of lithium oxide on top of elemental lithium. Since low recycling in LTX was achieved with similar coatings, we expect that hydrogen uptake by both lithium oxide and lithium must have been responsible for achieving lowered recycling. Indeed, it has been demonstrated in offline experiments that hydrogen uptake capability of lithium and lithium oxide are comparable [21].

References

[1] G. F. Matthews *et al.*, "The second phase of JET operation with the ITER-like wall," *Phys. Scr.*, vol. T159, Apr. 2014, Art. no. 014015.

[2] D. Mansfield *et al.*, "Enhancement of Tokamak fusion test reactor performance by lithium conditioning," *Phys. Plasmas*, vol. 3, no. 5, pp. 1892–1897, 1996, doi: 10.1063/1.871984.

[3] H. W. Kugel *et al.*, "The effect of lithium surface coatings on plasma performance in the national spherical torus experiment," *Phys. Plasmas*, vol. 15, May 2008, Art. no. 056118-1, doi: 10.1063/1.2906260.

[4] R. Majeski *et al.*, "Enhanced energy confinement and performance in a low-recycling tokamak," *Phys. Rev. Lett.*, vol. 97, no. 7, 2006, Art. no. 075002, doi: 10.1103/PhysRevLett.97.075002.

[5] G. Zuo *et al.*, "Primary results of lithium coating for the improvement of plasma performance in EAST," *Plasma Sci. Technol.*, vol. 12, no. 6, pp. 646–650, Dec. 2010. [Online]. Available: http://stacks.iop.org/1009-0630/12/i=6/a=02

[6] R. Kaita *et al.*, "Hydrogen retention in lithium on metallic walls from in vacuo analysis in LTX and implications for high-Z plasma-facing components in NSTX-U," *Fusion Eng. Des.*, vol. 117, pp. 135–139, 2017. [Online]. Available: http://www.sciencedirect.com/science/article/pii/S0920379616304574

[7] J. C. Schmitt *et al.*, "High performance discharges in the lithium tokamak experiment with liquid lithium walls," *Phys. Plasmas*, vol. 22, no. 5, 2015, Art. no. 056112. [Online]. Available: https://aip.scitation.org/doi/abs/10.1063/1.4921153

[8] D. P. Boyle *et al.*, "Observation of flat electron temperature profiles in the lithium tokamak experiment," *Phys. Rev. Lett.*, vol. 119, Jul. 2017, Art. no. 015001. [Online]. Available: https://link.aps.org/doi/10.1103/PhysRevLett.119.015001

[9] M. Lucia *et al.*, "Dependence of LTX plasma performance on surface conditions as determined by in situ analysis of plasma facing components," *J. Nucl. Mater.*, vol. 463, pp. 907–910, Aug. 2015. [Online]. Available: http://www.sciencedirect.com/science/article/pii/S0022311514007879

[10] M. Lucia, "Material surface characteristics and plasma performance in the lithium Tokamak experiment," Ph.D. dissertation, Princeton Plasma Phys. Lab., Princeton Univ., Princeton, NJ, USA, 2015.

[11] J. Hoenigman and R. Keil, "An XPS study of the adsorption of oxygen and water vapor on clean lithium films," *Appl. Surf. Sci.*, vol. 18, nos. 1–2, pp. 207–222, May 1984. [Online]. Available: http://www.sciencedirect.com/science/article/pii/037859638490045X

[12] R. Sullenberger, "Uptake and retention of residual vacuum gases in lithium and lithium films," M.S. thesis, Aerosp. Eng., Princeton Univ., Princeton, NJ, USA, 2012.

[13] D. Elliott, "Initial results from the newly upgraded ltx-β," presented at the Conf. Symp. Fusion Eng., 2019.

[14] M. Ohring, "Chapter 3," in *Materials Science of Thin Films*, 2nd ed, M. Ohring, Ed. San Diego, CA, USA,: Academic, 2002, pp. 95–144. [Online]. Available: http://www.sciencedirect.com/science/article/pii/B9780125249751500069

[15] A. Maan *et al.*, "A simple vacuum suitcase for plasma facing component characterization in fusion devices," *Rev. Sci. Instrum.*, vol. 91, 2020, doi: 10.1063/1.5119166.

[16] F. Bedoya, J. Allain, F. Scotti, B. Labombard, R. Kaita, and P. Krstic, "Effect of boronization on plasma-facing graphite surfaces and its correlation with the plasma behavior in NSTX-U," *Nucl. Mater. Energy*, vol. 17, pp. 211–216, Dec. 2018. [Online]. Available: http://www.sciencedirect.com/science/article/pii/S2352179118300929

[17] A. C. Kozen *et al.*, "Atomic layer deposition and *in situ* characterization of ultraclean lithium oxide and lithium hydroxide," *J. Phys. Chem. C*, vol. 118, no. 48, pp. 27749–27753, Dec. 2014, doi: 10.1021/jp509298r.

[18] K. N. Wood and G. Teeter, "XPS on li-battery-related compounds: Analysis of inorganic SEI phases and a methodology for charge correction," *ACS Appl. Energy Mater.*, vol. 1, no. 9, pp. 4493–4504, Sep. 2018, doi: 10.1021/acsaem.8b00406.

[19] *NIST X-ray Photoelectron Spectroscopy Database, Version 4.1*, Nat. Inst. Standards Technol., Gaithersburg, MA, USA, 2012.

[20] K. Kanamura, H. Tamura, and Z.-I. Takehara, "XPS analysis of a lithium surface immersed in propylene carbonate solution containing various salts," *J. Electroanal. Chem.*, vol. 333, nos. 1–2, pp. 127–142, Jul. 1992. [Online]. Available: http://www.sciencedirect.com/science/article/pii/002207289280386I

[21] L. Buzi *et al.*, "Hydrogen retention in lithium and lithium oxide films," *J. Nucl. Mater.*, vol. 502, pp. 161–168, Apr. 2018.

Plasma Facing Component Characterization and Correlation With Plasma Conditions in Lithium Tokamak Experiment-β

Anurag Maan, Evan Ostrowski, Robert Kaita, David Donovan, Richard Majeski, Dennis Boyle, Paul Hughes, Enrique Merino, Tom Kozub, Bruce E. Koel, Drew Elliott, Theodore Biewer, Filippo Scotti, Vsevolod Soukhanovskii, and Robert Lunsford

***Abstract*— Lithium coatings in the Lithium Tokamak eXperiment (LTX) led to flat temperature profiles. The flat temperature profiles were observed along with a hot, low density edge, implying a broad, collisionless scrape-off layer (SOL). Additionally, in vacuo X-ray photoelectron spectroscopy (XPS) measurements established that lithium coatings evaporatively deposited onto high-Z plasma facing components (PFCs) became oxidized while retaining the ability to achieve good plasma performance long after lithium was applied to the PFCs. Longstanding theory predicted flat temperature profiles with low recycling walls, which was presumed to be due to hydrogen binding with elemental lithium to form lithium hydride. The presence of oxidized lithium, however, raised questions regarding the exact mechanism of hydrogen retention in LTX. To investigate these questions, the upgraded facility LTX-β includes a new sample exposure probe (SEP) for more detailed in vacuo analysis of PFC samples. The SEP is equipped with a vacuum suitcase capable of transporting samples representative of the LTX-β outer midplane PFCs to a stand-alone XPS system while maintaining pressures lower than the LTX-β base vacuum to limit the contamination between sample exposure and analysis. The low-energy resolution XPS system used in past experiments could only enable the determination of elemental percentages on the PFC sample surfaces. Because the new XPS system has higher energy resolution, it is more direct to assign chemical compounds to the measured binding energies. This capability has been confirmed by comparing XPS data from PFC test samples with measurements using a commercial high-resolution XPS system. Quartz crystal microbalances (QCMs) were used to quantify the thickness of the deposited lithium on the LTX-β PFCs. This article describes the application of the SEP to characterize the PFC surfaces using XPS and their relationship to plasma conditions.**

***Index Terms*— Lithium, plasma chemistry, plasma confinement, plasma diagnostics, tokamaks.**

Manuscript received July 19, 2019; revised January 2, 2020; accepted January 18, 2020. This work was supported by the U.S. DOE under Grant DE-AC02-09CH11466, Grant DE-AC05-00OR22725, Grant DE-AC52-07NA27344, and Grant DE-SC0019308. The review of this article was arranged by Senior Editor G. H. Neilson. *(Corresponding author: Anurag Maan.)*

Anurag Maan, Robert Kaita, and David Donovan are with the Department of Nuclear Engineering, University of Tennessee, Knoxville, TN 37996 USA (e-mail: amaan@vols.utk.edu).

Evan Ostrowski and Bruce E. Koel are with the Chemical and Biological Engineering, Princeton University, Princeton, NJ 08544 USA.

Richard Majeski, Dennis Boyle, Paul Hughes, Enrique Merino, Tom Kozub, and Robert Lunsford are with the Princeton Plasma Physics Laboratory, Princeton, NJ 08540 USA.

Drew Elliott and Theodore Biewer are with the Oak Ridge National Laboratory, Oak Ridge, TN 37831 USA.

Filippo Scotti and Vsevolod Soukhanovskii are with the Lawrence Livermore National Laboratory, Livermore, CA 94550 USA.

Color versions of one or more of the figures in this article are available online at http://ieeexplore.ieee.org.

Digital Object Identifier 10.1109/TPS.2020.2969115

I. Introduction

THE choice of materials for the first wall inside a tokamak, also called the plasma facing components (PFCs), has major engineering and physics implications for the overall design. Empirically, it has been shown that the use of high-Z PFCs lowers confinement in JET [1]. It has also been observed that the use of low-Z PFCs, especially lithium, improves plasma performance in various machines, including TFTR, NSTX, CDX-U, and EAST [2]–[6]. One of the primary objectives of the Lithium Tokamak eXperiment (LTX) and its upgrade LTX-β is to investigate lithium as a PFC coating on a high-Z substrate in order to improve plasma performance. LTX is a spherical tokamak at the Princeton Plasma Physics Laboratory (PPPL) with a cylindrical vacuum vessel of dimensions 0.9 m height and 1.4 m inner diameter. Inside the vessel are stainless-steel-clad copper shells designed to be conformal to a plasma with major radius $R = 0.4$ m, minor radius $a = 0.26$ m (aspect ratio $A = 1.6$), and maximum elongation $\kappa \approx 1.5$ [7]. LTX operated with a toroidal field ≈ 1.7 kG, $I_p \leq 80$ kA, and a short duration of ≤ 25 ms. The facility was upgraded to LTX-β with nearly double the field and the addition of a neutral beam.

During its final campaign, LTX was fueled by gas puffs from the high field side. Once the fueling was terminated, Thomson Scattering measurements showed that the electron temperature profiles flattened. Although recycling was not measured directly, pressure measurement of the fueling gas before, during, and after the discharge indicated significant wall retention [8]. The LTX results were the first experimental observation of near-zero temperature gradient profiles attributed to low recycling PFCs. In addition, experimentally measured energy confinement exceeded the predictions for ohmic plasmas by a factor of $\sim$3 [8].

The materials analysis and particle probe (MAPP), designed to characterize PFC surfaces in vacuo (i.e., without any exposure to air) was first used on LTX. The samples were inserted to be flush with the plasma facing surfaces of the conducting

shells [9], [10]. Samples on the probe head included those made of stainless steel (SS-304 and SS-316) to match the LTX shell surfaces. The LTX shells and samples were then coated with lithium, after which the probe head was exposed to LTX plasma. Post exposure, the probe was retracted in vacuo into the MAPP analysis chamber for X-ray photoelectron spectroscopy (XPS) determination of the surface composition of the lithium coated SS-304 MAPP sample. XPS indicated an increase in the oxygen concentration of the sample after exposure to LTX residual vacuum conditions, which was attributed to oxidation by water vapor that was observed by the residual gas analyzer (RGA).

The temporal evolution of lithium and oxygen concentrations were also tracked using MAPP. It was observed that the Li(1s)/O(1s) ratio decreased, until it saturated the XPS probe depth, within 5 h [9], [10]. Beyond that, there was no observable change in the elemental concentration until 100 h, after which the Li(1s)/O(1s) ratio began to decrease slowly. The saturation of the ratio of lithium to oxygen to about 2:1 was attributed to the growth of Li_2O on freshly deposited lithium in the presence of residual water vapor, consistent with laboratory experiments [11], [12]. Specifically, below 100 Langmuirs (1 $L = 10^{-6}$ torr·s) of H_2O exposure, Li_2O forms preferentially on a clean lithium surface, while at higher exposures there is a transition to LiOH formation. For LTX-relevant water partial pressures, 100 L is equivalent to 14 h of exposure to residual vacuum. It was also observed that the presence of the oxide did not degrade plasma performance; LTX continued to get high plasma currents until 40 days after lithium deposition [6].

About 0.5 s after the plasma extinguished in LTX, the fast ion gauge showed a ∼60% reduction in H_2 inventory compared to calibration gas puffs where plasma was not initiated [6], [8]. Over longer (>10 s) timescales, however, the H_2 reading from the RGA for shots when plasma was initiated exceeded the recorded measurement for the calibrated gas puffs. This led to the conclusion that while a significant portion of hydrogen was retained in the PFCs during a plasma, the hydrogen out-gassed over time scales much longer than the plasma duration [6]. With 60% of an LTX relevant fluence of hydrogen fuel retained in a lithium coating of 100 nm, the Li coating should saturate with hydrogen in <10 shots (assuming Li:H = 1:1). However, this was not the case. Neither H retention nor plasma performance decayed after a few shots, but rather after 40 days and close to one hundred shots or more. This led to the conclusion that hydrogen was retained by lithium-coated PFCs in LTX such that it was free to diffuse out between shots. The conclusions regarding the state of the PFC using MAPP results were arrived at using elemental abundances only. Binding energy shifts using XPS can be used to identify chemical states, but MAPP did not have the energy resolution to identify different Li compounds that formed on the PFCs.

II. Upgrade to LTX-β

The upgrade to LTX-β included the ability to operate at higher fields and with more efficient Li evaporators

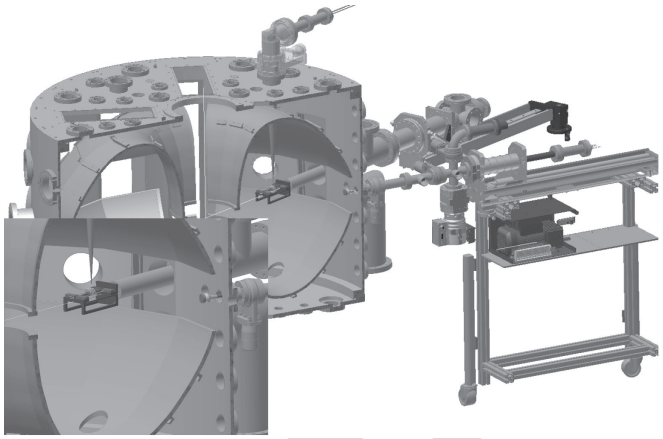

Fig. 1. CAD section view of the evaporator inserted to the central poloidal location, the SEP, and the QCM above the LTX-β vacuum vessel. Also visible are the stainless-steel-clad copper shells inside the vacuum vessel. Inset: zoomed-in view of the evaporator subassembly and trajectory of lithium vapor toward the QCM.

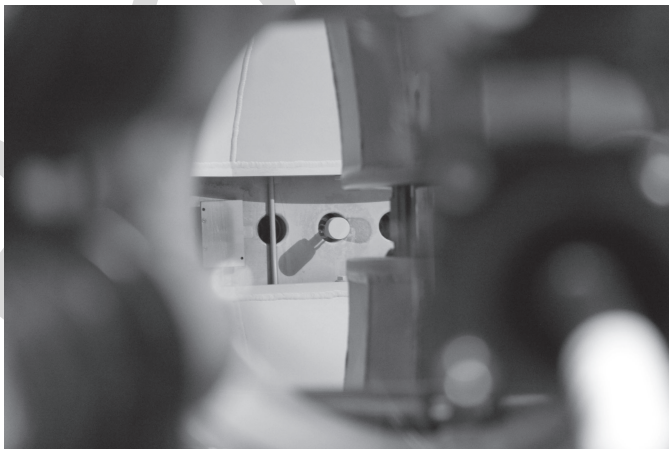

Fig. 2. SEP probe head immediately after lithium evaporation. The probe head face is flush with the inner face of the LTX-β shells. Two shadows from the SEP probehead are visible, the shadow to the bottom-left of the probe is cast by an in-vessel filament that is illuminating the vessel interior, the shadow to the right is cast by the lithium evaporator.

(see Fig. 1). The machine has been operated with 600 kW of neutral beam injection and several hundred nanometers of lithium coatings [13]. Fig. 3 illustrates the main plasma parameters of a wide variety of discharges through the upgrade campaign. It was observed that the discharges grew longer and had higher plasma current after lithium evaporation. In Fig. 3, lithium PFC discharges are divided into two groups. Discharges after the first lithium evaporation (represented by green bubbles in Fig. 3) had higher electron density, but were shorter in duration with lower plasma current. Discharges after subsequent lithium evaporations (represented by red bubbles in Fig. 3) could achieve longer durations and higher currents. Spectroscopic data indicated a reduction in carbon and oxygen impurities and an increase in lithium line emission when discharges were initiated after a fresh coat of lithium [13].

Each of the LTX-β lithium evaporators consists of a basket made of stainless steel mesh, suspended through two yttria

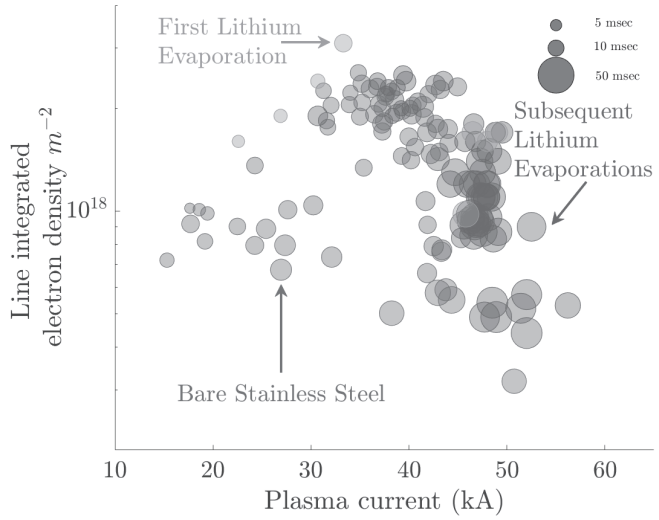

Fig. 3. Line integrated electron density as a function of plasma current for LTX-β discharges; bubble size is proportional to plasma current flat-top duration of 4–40 ms. Discharges with bare stainless steel walls are shown in blue; discharges after the first lithium evaporation are shown in green, and after subsequent lithium evaporations are shown in red.

TABLE I
CHRONOLOGY OF LITHIUM EVAPORATION EVENTS ON LTX-β

Days*	Li thickness QCM (nm)	Estimated Li on SEP (nm)
30.6	22	89.5
31.7	7	28.5
37.5	108	439.5
41.8	50.8	206.7
44.5	40	162.8

*Days from the first XPS measurement as referred in Fig 4.

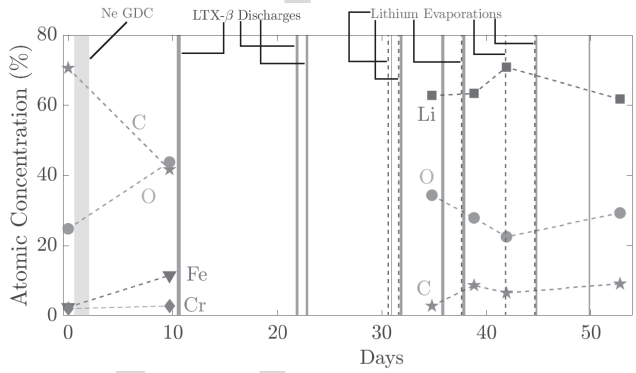

Fig. 4. Elemental concentrations measured using the SEP. Vertical green bar: neon glow discharge duration. Vertical blue bars: time duration over which LTX-β discharges were initiated. Dashed red lines: lithium evaporations on the shells and SEP.

rods for support. Evaporator temperatures are measured with a Type-K thermocouple inserted into one of the yttria rods [13]. The basket is surrounded by a tungsten coil heater that can be quickly ramped up to 60 A (∼500 W) to radiatively heat the lithium pieces loaded in the basket. The lithium pieces are pre-cut and loaded into a stainless steel container in an argon glovebox for transfer under argon. Lithium evaporators are back-filled with dry argon and lithium coupons carefully transferred into the evaporator from the container. A slight outflow of argon from the evaporator assembly is maintained, thereby minimizing the exposure of lithium to the atmosphere. LTX-β has two evaporators installed in diametrically opposite toroidal locations to provide near full coverage of PFCs by lithium coatings. Once lithium is loaded, the evaporators are pumped out and inserted into LTX-β, such that they are at the center of their respective poloidal planes as shown in Fig. 1. Each evaporator is situated under a shell penetration that provides a line of sight to a quartz crystal microbalance (QCM). The QCMs are used to keep track of lithium deposited per evaporation.

Simultaneously, the sample exposure probe (SEP) is inserted to be flush with the plasma facing side of the shells (see Fig. 2). The SEP is left in this position for lithium evaporations and subsequent plasma discharges. This article analyzes five such lithium evaporation events (Table I). The lithium deposited per evaporation is recorded by the QCM; these recorded values can be used to estimate the thickness of lithium deposited on the SEP using the expressions for evaporative flux [14]. Assuming the evaporator sub-assembly to be a point source, the lithium thickness on the SEP can be estimated by (1), where t_{SEP} is the thickness of lithium on the SEP, t_{QCM} is the lithium thickness measured by the QCM, θ is the angle from the point source to the SEP surface normal, r_{QCM} is the distance from the QCM to the evaporator source and r_{SEP} is the distance of the evaporator source to the SEP

$$t_{\mathrm{SEP}} = t_{\mathrm{QCM}} \cos(\theta) \frac{r_{\mathrm{QCM}}^2}{r_{\mathrm{SEP}}^2}. \quad (1)$$

Once the desired exposure of residual vacuum or plasma discharges is achieved, the SEP is removed from LTX-β and moved to the Surface Science and Technology Laboratory (SSTL) at PPPL where it is docked to an ultrahigh vacuum (UHV) system that has a XPS spectrometer [15]. The transfer is made within a limited time (<1.5 h), such that the fluence of impurities on the surface is similar to a MAPP scan [15].

III. ENHANCED SURFACE ANALYSIS CAPABILITIES

Prior to the introduction of lithium, surface conditioning for LTX-β involved Ne glow discharge conditioning (GDC) and simultaneous high temperature shell's bake at 250 °C. To ensure that the SEP sample head accurately represented the LTX plasma facing shells, the SEP was inserted flush with shells during GDC and bake and was maintained at the same temperature as the shells. Surface elemental composition was measured using XPS before and after the GDC (see Fig. 4). It was observed that the elemental concentration of C declined while the concentrations of Fe and O went up; this is attributed to the sputtering of the adventitious carbon by Ne, which would result in the underlying iron oxides to appear more intense on the XPS scan. The sampling depth is expected to be about 6 nm [15]. For these measurements, the SEP is left exposed inside LTX-β except for the brief intervals during which it is taken off for taking XPS scans. Following the first lithium evaporation and subsequent LTX-β discharges, surface

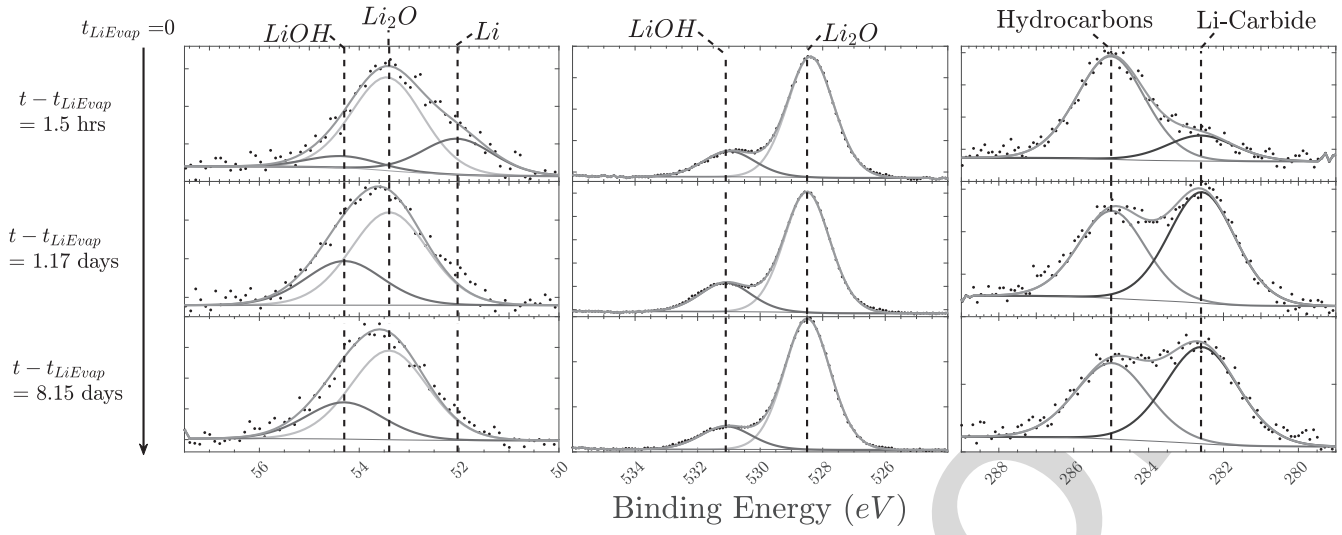

Fig. 5. Narrow band regional XPS scans for Li(1s), O(1s), and C(1s) along with probable fits are shown in left, middle, and right columns, respectively. The scans are arranged row-wise in increasing order of time from a lithium evaporation.

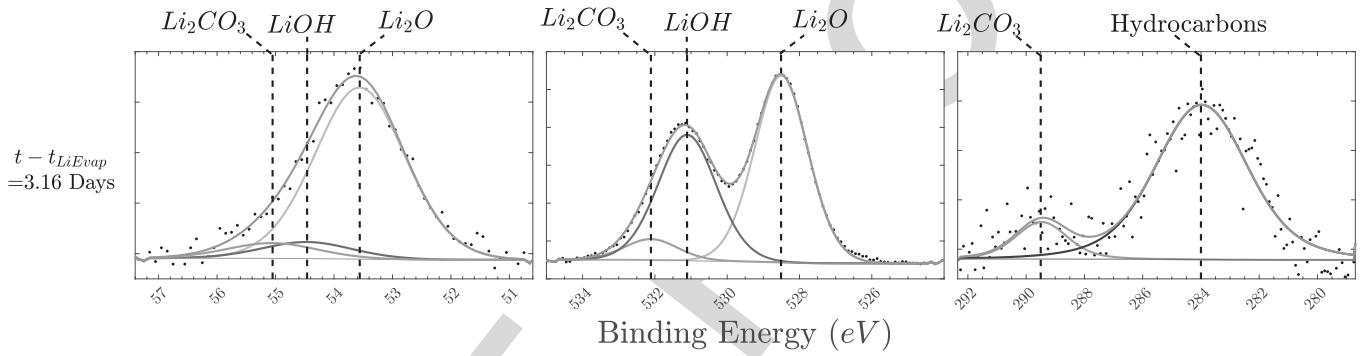

Fig. 6. Narrow-band regional XPS scans along with probable fits for Li(1s), O(1s), and C(1s) are shown in left, middle, and right columns, respectively. The scan was taken 3.16 days after lithium was deposited on bare stainless steel walls and sample head of the SEP.

concentrations were measured again; the measurements show that the stainless steel substrate of the SEP was completely covered by lithium. XPS measurements made for relatively fresh lithium coatings show higher Li and lower O concentrations; as the surface accumulates LTX-β residual vacuum exposure time, the O concentration seems to climb up, and Li concentration is seen to decrease relative to O.

A. Surface Chemical Species Identification Using the SEP

Coupled with the XPS system at SSTL, the SEP enabled chemical identification of species present on the surface. Figs. 5 and 6 represent the regional narrow band scans collected for the samples whose elemental compositions are shown in Fig. 4. Similar studies have been performed for boronized NSTX-U PFCs [16] and have enabled identification of oxygen retention mechanisms that resulted in improved plasma performance.

The O(1s) peak, shown in the middle column of Fig. 5, exhibited two features that were identified to be Li_2O and LiOH at the binding energies of 528.5 and 531.1 eV, respectively. The absolute values of these binding energies and the difference between them is consistent with results cited elsewhere [17], [18]. The O(1s) Li_2CO_3 peak was identified to be at 532.1 eV [17]–[19] for measurements that were taken after the first application of lithium on steel PFCs of LTX-β (see Fig. 6). All peaks are referenced to a hydrocarbon peak in the C(1s) region at 285 eV. An additional feature in the C(1s) region at 282.6 eV is attributed to lithium carbide with reference to the hydrocarbon peak at 285 eV; this assignment is consistent with values in the literature [20]. The higher energy feature in the C(1s) region visible in Fig. 6 at 289.4 eV is attributed to Li_2CO_3. The Li(1s) region in both Figs. 5 and 6 was fit with peaks at 52.03, 53.4, 54.3, and 55 eV for Li, Li_2O, LiOH, and Li_2CO_3, respectively. The difference in binding energies of these fits was forced to be consistent with values reported in the literature [12], [17], [19].

The narrow region scans elaborate on the richness of surface chemistry of evaporative lithium coatings on PFCs. The surface chemistry is both a function of tokamak residual vacuum and plasma exposures and is expected to be similar across machines that employ lithium coatings. However, the rate of growth of these species will be dependent on each machine's residual vacuum and plasma exposure conditions. The O(1s) region indicates that the primary lithium species on the PFCs is Li_2O followed by LiOH. The first application of lithium,

as shown in Fig. 6, however, appears to result in the formation of Li_2CO_3 and LiOH in addition to Li_2O, and this was observed along with plasma performance that was moderate in comparison to performance after a few more evaporations, as witnessed by an increase in plasma current and density (see Fig. 3). This is likely a result of vacuum and PFC surface conditions being different from samples represented in Fig. 5, for which lithium was evaporated on already lithiated PFCs. The carbonate production is likely a result of adventitious carbon on the stainless steel surface, which although reduced in magnitude after GDC, was still amongst the two largest elemental constituents of the steel PFCs.

Two novel observations can be made about lithium PFCs that consist of evaporative lithium coatings. First is the formation and growth of lithium carbide, as can be seen in the C(1s) regional scan in Fig. 5. The second is the presence of a relatively large elemental lithium peak in row 1 and column 1 of Fig. 5. The presence of elemental lithium indicates that the oxide grows on top of lithium deposited during evaporation events.

IV. Conclusion

The chemical evolution of lithium coated evaporatively on stainless steel PFCs was tracked through surface conditioning, lithium deposition, and plasma discharge events. This was made possible due to a SEP that enabled the UHV transfer of samples to a dedicated XPS system with resolution that was sufficient to identify chemical species. The results support the hypothesis that for evaporative coatings of lithium under low-water content residual vacuum, Li_2O grows before transitioning to LiOH. We further hypothesize that the first few lithium evaporations of a few hundred nanometers in total on LTX-β shells were able to limit carbon uptake in subsequent lithium coatings from underlying stainless steel. The first lithium coating consisted of relatively large hydroxide and carbonate components in addition to Li_2O. The hydroxide and carbonate in the coating are likely a result of the interaction of lithium from the first deposition with the underlying carbon and oxygen on the steel. Subsequent lithium evaporations likely bury these species such that these later coatings manifest as mostly Li_2O on lithium. The presence of elemental lithium seen in freshly deposited lithium coatings indicates limited oxygen codeposition with lithium and hint at an ordered growth of lithium oxide on top of elemental lithium. Since low recycling in LTX was achieved with similar coatings, we expect that hydrogen uptake by both lithium oxide and lithium must have been responsible for achieving lowered recycling. Indeed, it has been demonstrated in offline experiments that hydrogen uptake capability of lithium and lithium oxide are comparable [21].

References

[1] G. F. Matthews *et al.*, "The second phase of JET operation with the ITER-like wall," *Phys. Scr.*, vol. T159, Apr. 2014, Art. no. 014015.

[2] D. Mansfield *et al.*, "Enhancement of Tokamak fusion test reactor performance by lithium conditioning," *Phys. Plasmas*, vol. 3, no. 5, pp. 1892–1897, 1996, doi: 10.1063/1.871984.

[3] H. W. Kugel *et al.*, "The effect of lithium surface coatings on plasma performance in the national spherical torus experiment," *Phys. Plasmas*, vol. 15, May 2008, Art. no. 056118-1, doi: 10.1063/1.2906260.

[4] R. Majeski *et al.*, "Enhanced energy confinement and performance in a low-recycling tokamak," *Phys. Rev. Lett.*, vol. 97, no. 7, 2006, Art. no. 075002, doi: 10.1103/PhysRevLett.97.075002.

[5] G. Zuo *et al.*, "Primary results of lithium coating for the improvement of plasma performance in EAST," *Plasma Sci. Technol.*, vol. 12, no. 6, pp. 646–650, Dec. 2010. [Online]. Available: http://stacks.iop.org/1009-0630/12/i=6/a=02

[6] R. Kaita *et al.*, "Hydrogen retention in lithium on metallic walls from in vacuo analysis in LTX and implications for high-Z plasma-facing components in NSTX-U," *Fusion Eng. Des.*, vol. 117, pp. 135–139, 2017. [Online]. Available: http://www.sciencedirect.com/science/article/pii/S0920379616304574

[7] J. C. Schmitt *et al.*, "High performance discharges in the lithium tokamak experiment with liquid lithium walls," *Phys. Plasmas*, vol. 22, no. 5, 2015, Art. no. 056112. [Online]. Available: https://aip.scitation.org/doi/abs/10.1063/1.4921153

[8] D. P. Boyle *et al.*, "Observation of flat electron temperature profiles in the lithium tokamak experiment," *Phys. Rev. Lett.*, vol. 119, Jul. 2017, Art. no. 015001. [Online]. Available: https://link.aps.org/doi/10.1103/PhysRevLett.119.015001

[9] M. Lucia *et al.*, "Dependence of LTX plasma performance on surface conditions as determined by in situ analysis of plasma facing components," *J. Nucl. Mater.*, vol. 463, pp. 907–910, Aug. 2015. [Online]. Available: http://www.sciencedirect.com/science/article/pii/S0022311514007879

[10] M. Lucia, "Material surface characteristics and plasma performance in the lithium Tokamak experiment," Ph.D. dissertation, Princeton Plasma Phys. Lab., Princeton Univ., Princeton, NJ, USA, 2015.

[11] J. Hoenigman and R. Keil, "An XPS study of the adsorption of oxygen and water vapor on clean lithium films," *Appl. Surf. Sci.*, vol. 18, nos. 1–2, pp. 207–222, May 1984. [Online]. Available: http://www.sciencedirect.com/science/article/pii/037859638490045X

[12] R. Sullenberger, "Uptake and retention of residual vacuum gases in lithium and lithium films," M.S. thesis, Aerosp. Eng., Princeton Univ., Princeton, NJ, USA, 2012.

[13] D. Elliott, "Initial results from the newly upgraded ltx-β," presented at the Conf. Symp. Fusion Eng., 2019.

[14] M. Ohring, "Chapter 3," in *Materials Science of Thin Films*, 2nd ed, M. Ohring, Ed. San Diego, CA, USA,: Academic, 2002, pp. 95–144. [Online]. Available: http://www.sciencedirect.com/science/article/pii/B9780125249751500069

[15] A. Maan *et al.*, "A simple vacuum suitcase for plasma facing component characterization in fusion devices," *Rev. Sci. Instrum.*, vol. 91, 2020, doi: 10.1063/1.5119166.

[16] F. Bedoya, J. Allain, F. Scotti, B. Labombard, R. Kaita, and P. Krstic, "Effect of boronization on plasma-facing graphite surfaces and its correlation with the plasma behavior in NSTX-U," *Nucl. Mater. Energy*, vol. 17, pp. 211–216, Dec. 2018. [Online]. Available: http://www.sciencedirect.com/science/article/pii/S2352179118300929

[17] A. C. Kozen *et al.*, "Atomic layer deposition and *in situ* characterization of ultraclean lithium oxide and lithium hydroxide," *J. Phys. Chem. C*, vol. 118, no. 48, pp. 27749–27753, Dec. 2014, doi: 10.1021/jp509298r.

[18] K. N. Wood and G. Teeter, "XPS on li-battery-related compounds: Analysis of inorganic SEI phases and a methodology for charge correction," *ACS Appl. Energy Mater.*, vol. 1, no. 9, pp. 4493–4504, Sep. 2018, doi: 10.1021/acsaem.8b00406.

[19] *NIST X-ray Photoelectron Spectroscopy Database, Version 4.1*, Nat. Inst. Standards Technol., Gaithersburg, MA, USA, 2012.

[20] K. Kanamura, H. Tamura, and Z.-I. Takehara, "XPS analysis of a lithium surface immersed in propylene carbonate solution containing various salts," *J. Electroanal. Chem.*, vol. 333, nos. 1–2, pp. 127–142, Jul. 1992. [Online]. Available: http://www.sciencedirect.com/science/article/pii/002207289280386I

[21] L. Buzi *et al.*, "Hydrogen retention in lithium and lithium oxide films," *J. Nucl. Mater.*, vol. 502, pp. 161–168, Apr. 2018.